JACS
JOURNAL OF THE AMERICAN CHEMICAL SOCIETY
Article
pubs.acs.org/JACS

Three-Mode Electrochemical Sensing of Ultralow MicroRNA Levels

Mahmoud Labib,[†] Nasrin Khan,[†] Shahrokh M. Ghobadloo,[†] Jenny Cheng,[‡] John Paul Pezacki,[†,‡] and Maxim V. Berezovski*[,†]

[†]Department of Chemistry, University of Ottawa, 10 Marie Curie, Ottawa, Ontario K1N 6N5, Canada
[‡]Steacie Institute for Molecular Sciences, National Research Council of Canada, 100 Sussex Drive, Ottawa, Ontario K1A 0R6, Canada

Supporting Information

ABSTRACT: MicroRNAs (miRNAs) are an emerging class of biomarkers that are frequently deregulated in cancer cells and have shown great promise for cancer classification and prognosis. In this work, we developed a three-mode electrochemical sensor for detection and quantitation of ultralow levels of miRNAs in a wide dynamic range of measured concentrations. The sensor facilitates three detection modalities based on hybridization (H-SENS), p19 protein binding (P-SENS), and protein displacement (D-SENS). The combined three-mode sensor (HPD-SENS) identifies as low as 5 aM or 90 molecules of miRNA per 30 μL of sample without PCR amplification, and can be operated within the dynamic range from 10 aM to 1 μM. The HPD sensor is made on a commercially available gold nanoparticles-modified electrode and is suitable for analyzing multiple miRNAs on a single electrode. This three-mode sensor exhibits high selectivity and specificity and was used for sequential analysis of miR-32 and miR-122 on one electrode. In addition, the H-SENS can recognize miRNAs with different A/U and G/C content and distinguish between a fully matched miRNA and a miRNA comprising either a terminal or a middle single base mutation. Furthermore, the H- and P-SENS were successfully employed for direct detection and profiling of three endogenous miRNAs, including hsa-miR-21, hsa-miR-32, and hsa-miR-122 in human serum, and the sensor results were validated by qPCR.

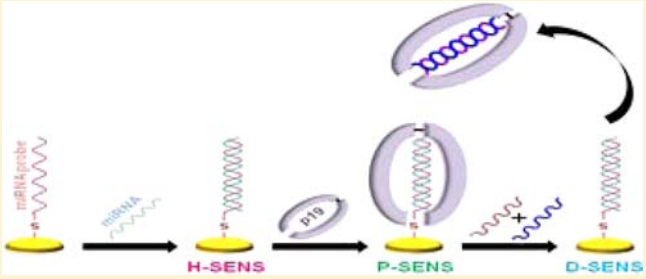

INTRODUCTION

Disease diagnosis on the basis of biomolecular analysis requires rapid, sensitive, and cost-effective assays.[1,2] As nucleic acids are important biomarkers for disease diagnosis, their detection has brought a great deal of attention to the development of nucleic acids biosensors.[3,4] MicroRNAs (miRNAs) are an abundant class of small RNAs regulating the expression of at least one-third of all human genes.[5,6] They are involved in tumor metastasis,[7] stem-cell differentiation and renewal,[8] and viral replication.[9] MicroRNAs are also an emerging class of diagnostic markers that can signify the presence of diseases and can be employed to predict its course.[10,11] MicroRNAs have been found in blood serum, plasma, urine, saliva, and other body fluids. Once thought of as unstable RNA molecules, circulating miRNAs are in fact highly stable in blood inside microparticles and exosomes or in a complex with an RNA binding protein, Nucleophosmin1.[12] The expression profiles of circulating miRNAs are correlated with various diseases, including cancer,[13] diabetes,[14] and tissue injury after stroke.[15] Therefore, these circulating miRNAs are utilized as minimally invasive biomarkers in diagnosis and monitoring of human cancers.[16]

Detection of miRNAs is challenging because of their short and highly homologous sequences (single base differences), low concentrations and wide dynamic range (from 0 to 1 pM of miRNAs in human serum), large variation in base composition (G/C or A/T rich), and its secondary structure. PCR-based methods exhibit variations with increasing cycle number and require amplification.[17] Recently, our group has reported a protein-facilitated affinity capillary electrophoresis (ProFACE) assay with laser-induced fluorescent detection (LIF) which allowed the detection of as low as 0.5 fM of miRNA.[18] This homogeneous assay was based on the unique binding property of p19 RNA binding protein from carnation Italian ring spot virus (p19) to small 21−23 bp dsRNA with nanomolar affinity.[19] The binding between p19 and dsRNAs occurs *via* electrostatic and hydrogen-bonding interactions between the β-sheet formed by the p19 homodimer and the sugar−phosphate backbone of dsRNA, thereby making its binding sequence-independent of the RNA substrate. Remarkably, p19 protein does not bind to ssRNA, rRNA, mRNA, ssDNA, or dsDNA.[20]

In the present study, we further exploited the strong and nonsequence specific binding of a p19 fused dimer protein to double stranded miRNAs and developed a three-mode electrochemical sensor (HPD-SENS) for analysis of five miRNAs. These miRNAs include miR-21, miR-32, miR-122, miR-141, and miR-200 which have been reported as biomarkers for colorectal,[21] prostate,[22] liver,[23] colon,[24] and ovarian tumors,[25] respectively. We reached an extremely low limit of

Received: August 18, 2012
Published: January 30, 2013

   dx.doi.org/10.1021/ja308216z | J. Am. Chem. Soc. 2013, 135, 3027−3038

detection down to ~90 molecules of miRNAs per 30 μL of sample in a broad dynamic range of miRNA concentrations extending from 10 aM to 1 μM, without any fluorescent labeling or PCR amplification. In addition, the sensor can recognize miRNAs with different A/U and G/C content and distinguish between a fully matched miRNA and a miRNA comprising either a terminal or a middle single base mutation. Finally, we profiled three endogenous hsa-miR-21, hsa-miR-32, and hsa-miR-122 in human serum.

EXPERIMENTAL SECTION

Sensor Preparation. Prior to experiments, the gold nanoparticle modified screen-printed carbon electrode (GNPs-SPCE) (L33 × W10 × H0.5, Dropsens, Spain) was washed thoroughly with deionized nuclease-free water and then dried with N_2. Subsequently, the electrode was incubated with 1 μM of the HPLC purified detection probe for miR-21 with the sequence $^{5'}$pUGCAACUUAGUAAUGUGCAAUA$^{3'}$-linker-SH, containing a phosphate group at the 5′ position (denoted with p) and modified at the 3′ position with a 6-hydroxyhexyl disulfide group in the incubation buffer, 25 mM phosphate buffer (pH 7.0) with 25 mM NaCl for 5 days at 4 °C. Finally, the electrode was incubated with 0.1 mM 2-mercaptoethanol in ethanol for 5 min to backfill the empty spots of the electrode surface, thus reducing the nonspecific adsorption onto the surface. All oligonucleotides used in the experiments were purchased from Integrated DNA Technologies.

Electrochemical Measurements. Electrochemical studies, including square wave voltammetry (SWV) and electrochemical impedance spectroscopy (EIS), were performed with an electrochemical analyzer (CH Instruments 660D, TX) connected to a personal computer. All measurements were carried out at room temperature in an enclosed and grounded Faraday cage. A conventional three-electrode configuration was printed on a ceramic substrate; including a GNPs-SPCE electrode as the working electrode, carbon counter electrode, and a silver pseudoreference electrode. A three-electric contacts edge connector (Dropsens, Spain) was used to connect the screen-printed electrode with the potentiostat. The open-circuit or rest-potential of the system was measured prior to all electrochemical experiments to prevent sudden potential-related changes in the self-assembled monolayer. SWV measurements were carried out in the range −400 to 800 mV with a step potential of 4 mV, amplitude of 5 mV, and frequency of 10 Hz. EIS measurements were conducted in the frequency range 100 kHz to 0.1 Hz, at a formal potential of 100 mV and AC amplitude of 5 mV. The measured EIS spectra were analyzed with the help of equivalent circuit using ZSimpWin 3.22 (Princeton Applied Research), and the data were presented in Nyquist plots. Electrochemical measurements were performed in the incubation buffer, containing 4 mM $K_3[Fe(CN)_6]$ and 10 μM $[Ru(NH_3)_6]Cl_3$. Importantly, all measurements were repeated for a minimum of three times with separate electrodes to obtain statistically meaningful results.

P19 Expression and Purification. Construction of the pTriEx-p19 plasmid encoding the codon-optimized carnation Italian ring spot virus p19 protein with a C-terminal octahistidine tag was previously reported.[26,27] Protein p19 is a molecularly engineered dimer made by linking two monomers with a peptide linker "GGGGSGGGGS" connecting the C-terminus of one monomer to the N-terminus of the other. Bacterial expression of the His-tagged p19 protein dimer was carried out as reported elsewhere,[26,27] with the following modifications. Briefly, *E. coli* strain BL21 (DE3) harboring the dimer p19−2X construct was cultivated in LB medium at 37 °C until an optical density of 0.5−0.6 was achieved at 600 nM (OD_{600}). Expression of the p19 protein was induced by 1 mM of isopropyl β-D-1-thiogalactopyranoside (IPTG, Sigma-Aldrich), and the bacterial culture was then grown for an additional 2−3 h at 28 °C until the OD_{600} reached 1−1.5. After centrifugation, bacterial pellets were resuspended in the lysis buffer (50 mM Tris−HCl, 300 mM NaCl, 10 mM imidazole, 1 mM dithiothreitol (DTT), and 1× complete protease inhibitor cocktail from Roche, pH 8) and lysed by sonication on an ice-bath. The cell lysate was then centrifuged at 20 000 *g* for 20 min at 4 °C. Afterward, the soluble lysate fraction containing the His-tagged p19 protein was loaded onto a HisTrap FF nickel affinity column (GE Healthcare). Subsequently, the column was washed with 10 column volumes of the wash buffer (50 mM Tris−HCl, 300 mM NaCl, 50 mM imidazole, pH 8). Elution of the His-tagged p19 protein was performed using the elution buffer (50 mM Tris−HCl, 300 mM NaCl, 250 mM imidazole, pH 8), where 10 mM DTT was added immediately to the eluate. The eluates were then combined and concentrated to 0.5 mL using the Amicon Ultra 10 kDa MWCO centrifugal filter device (Milipore, MA). Consequently, the concentrated eluate was additionally purified using Superdex-200 size-exclusion column chromatography (GE Healthcare) equilibrated with 20 mM Tris−HCl, 50 mM NaCl, 1 mM EDTA, 5 mM TCEP, pH 7.4 at a flow rate of 0.5 mL min^{-1}. Finally, fractions containing the purified p19 protein were analyzed by sodium dodecyl sulfate−polyacrylamide gel electrophoresis (SDS-PAGE), combined, and stored at 4 °C.

Sensor Preparation for Detection of Single Base Mutation and A/U and G/C Rich miRNAs. To assess the single base mismatch sensitivity of the developed sensor, 12 electrodes were incubated with 1 μM of the detection probe for miR-32 with the sequence $^{5'}$pUGCAACUUAGUAAUGUGCAAUA$^{3'}$-linker-SH in the incubation buffer for 5 days at 4 °C. Subsequently, the electrodes were incubated with 0.1 mM 2-mercaptoethanol in ethanol for 5 min. In order to test the ability of the sensor to detect A/U and G/C rich miRNAs, 12 sensors were prepared where the first six were incubated with 1 μM of the detection probe for A/U rich miRNA with the sequence $^{5'}$pUAAAACUUAGUAAUGUAUAAUA$^{3'}$-linker-SH, whereas the other six sensors were incubated with 1 μM of the detection probe for G/C rich miRNA with the sequence $^{5'}$pGGCCGCGUCGUAGUGUGCGGUG$^{3'}$-linker-SH in the incubation buffer for 5 days at 4 °C. Subsequently, the electrodes were incubated with 0.1 mM 2-mercaptoethanol in ethanol for 5 min.

Sensor Preparation for miRNA Profiling in Human Serum. There were 14 sensors prepared, where the first four were incubated with 1 μM of the detection probe for miR-21 with the sequence $^{5'}$pUCAACAUCAGUCUGAUAAGCUA$^{3'}$-linker-SH. Another set of four electrodes were incubated with 1 μM of the detection probe for miR-32 with the sequence $^{5'}$pUGCAACUUAGUAAUGUGCAAUA$^{3'}$-linker-SH. A third set of four electrodes were incubated with 1 μM of the detection probe for miR-122 with the sequence $^{5'}$pAACGCCAUUAUCACACUAAAUA$^{3'}$-linker-SH. One electrode was incubated with 1 μM of the detection probe for A/U rich miRNA with the sequence $^{5'}$pUAAAACUUAGUAAUGUAUAAUA$^{3'}$-linker-SH, whereas the other electrode was incubated with 1 μM of the detection probe for G/C rich miRNA with the sequence $^{5'}$pGGCCGCGUCGUAGUGUGCGGUG$^{3'}$-linker-SH. All probes were dissolved in the incubation buffer and incubated with the electrodes for 5 days at 4 °C. Subsequently, the electrodes were incubated with 0.1 mM 2-mercaptoethanol in ethanol for 5 min. Prior to experiments, 1 mL of human serum from healthy donor, pooled gender (Bioreclamation LLC, NY), was treated with 100 μL of 100 mg mL^{-1} yeast tRNA (Calbiochem, Germany), and then a serum aliquot was 10× diluted in the incubation buffer and heated for 15 min at 95 °C. Subsequently, the aliquot was incubated with each sensor containing an immobilized capture probe specific for either miR-21 or miR-32, miR-122 at 37 °C for 1 h. Four control experiments were performed; two of them were carried out by incubating each of the thee sensors with either 5.1 mg mL^{-1} HSA or 100 mg mL^{-1} yeast tRNA at 37 °C for 1 h followed by incubation with 10 μg mL^{-1} of p19 protein at 37 °C for 1 h in a dark humidity chamber. A third control experiment was performed by incubating the p19 protein directly with each of the three sensors under the same incubation conditions. A fourth control experiment was performed by incubating both electrodes containing the A/U and G/C rich probes with the serum aliquot followed by incubation with p19 protein under the same conditions.

RNA Extraction from Human Serum for qPCR. Human serum was thawed on ice. Afterward, β-mercaptoethanol was added to the lysis solution before mixing with the serum sample to guard against the

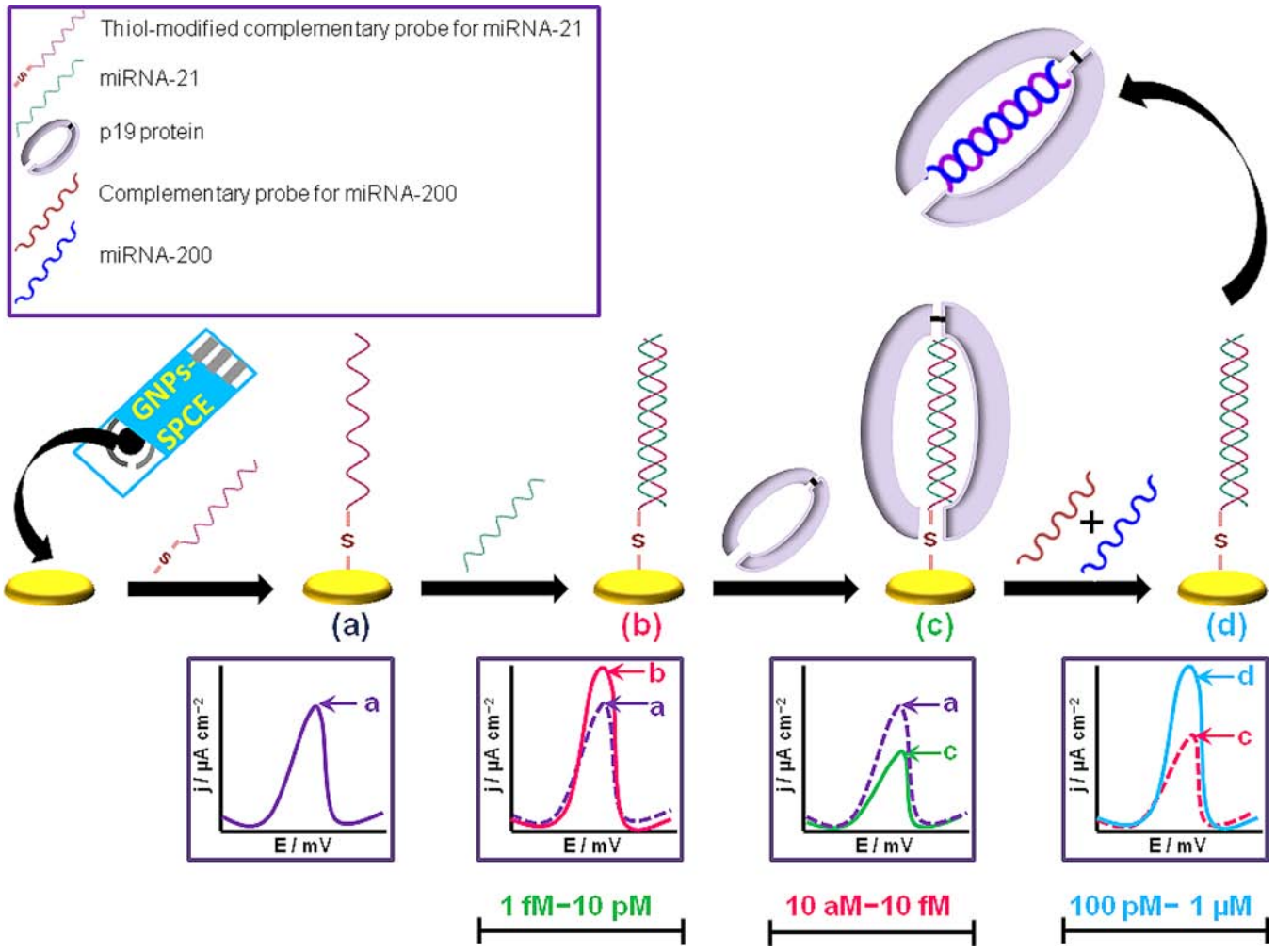

Figure 1. Schematic representation of the 3-mode electrochemical sensor (HPD-SENS) for detection of miRNAs. (a) A thiol-modified complementary probe for miR-21 was self-assembled onto a gold nanoparticles-modified screen-printed carbon electrode (GNPs-SPCE) followed by backfilling the surface with 0.1 mM 2-mercaptoethanol. (b) A hybridization-based sensor (H-SENS) where the binding of the target miR-21 caused an increase in the current intensity, measured by square wave voltammetry (SWV). The linear detection range of the H-SENS is from 1 fM to 10 pM. (c) A p19 protein-based sensor (P-SENS) where the binding of the p19 protein caused a large decrease in current density and thus improved the detection range. The linear detection range of the P-SENS is from 10 aM to 10 fM. (d) A displacement-based sensor (D-SENS) where the hybridization product of miR-200 and its complementary probe forced the p19 protein to dissociate from the previous immobilized hybrid, causing a shift-back in the signal. The linear detection range of the D-SENS is from 100 pM to 1 μM.

RNase activity. Subsequently, the total RNA was isolated using plasma/serum circulating RNA purification kit (Norgen BioTek Corp., Canada) according to the manufacturer's protocol. Briefly, a sample was mixed with approximately two sample volumes of the lysis solution and 0.2 mL of the separation matrix. Next, the mixture was vortexed for 30 s, followed by incubation at 60 °C for 10 min. Afterward, three volumes of 99% ethanol were added and mixed by vortexing for 30 s. Subsequently, the mixture was centrifuged using a swinging bucket rotor for 1 min at 300 RCF, and then carefully decanted in order to ensure that the slurry pallet was not dislodged. The binding solution was then added to the pellet, and incubated at 60 °C for 10 min. After adding 0.3 mL of 99% ethanol, the slurry was loaded onto a mini filter spin column. This was followed by washing of the bound RNA three times to remove the remaining proteins and other impurities. The purified total miRNA was then eluted in 60 μL RNase free water.

Quantitative Real-Time Polymerase Chain Reaction (qPCR) Experiments. Extracted total miRNAs (100 ng) were polyadenylated using poly A polymerase and ATP according to NCode miRNA first-strand cDNA synthesis kit instructions (Invitrogen). Next, 4 μL of each reaction was reverse transcribed to generate the first-strand cDNAs from the tailed miRNA populations, using Superscript-III reverse transcriptase and a specially designed universal reverse transcriptase primer, provided with the kit. Subsequently, the produced cDNAs were diluted 10 times in DEPC-treated water and used for qPCR experiments. Platinum SYBR green qPCR supermix-UDG reagent (MIRQ-100, Invitrogen, U.S.), miRNA-specific primers including a miR-21 forward primer: $^{5'}$ACACTCCAGCTGGG-TAGCTTATCAGACTGA$^{3'}$, miR-32 forward primer: $^{5'}$ACACTC-CAGCTGGGTATTGCACATTACTAA$^{3'}$, miR-122 forward primer: $^{5'}$ACACTCCAGCTGGGTGGAGTGTGACAATGG$^{3'}$, and a univer-sal qPCR primer: $^{5'}$TGGTGTCGTGGAGTCG$^{3'}$ were used to monitor the amount of target miRNAs. All reactions were monitored by a real-time PCR detection system (Bio-Rad CFX), using the following thermocycler conditions: 50 °C for 2 min, 95 °C for 2 min, 40 cycles at 95 °C for 3 s, and 55 °C for 30 s. The levels of hsa-miR-21, hsa- miR-32, and hsa-miR-122 in serum were measured on the basis of the standard curve obtained using a serial dilution of synthetic miR-32.

RESULTS AND DISCUSSION

Principle of the Three-Mode Electrochemical Sensor (HPD-SENS). A schematic representation of the sensor is

dx.doi.org/10.1021/ja308216z | J. Am. Chem. Soc. 2013, 135, 3027−3038

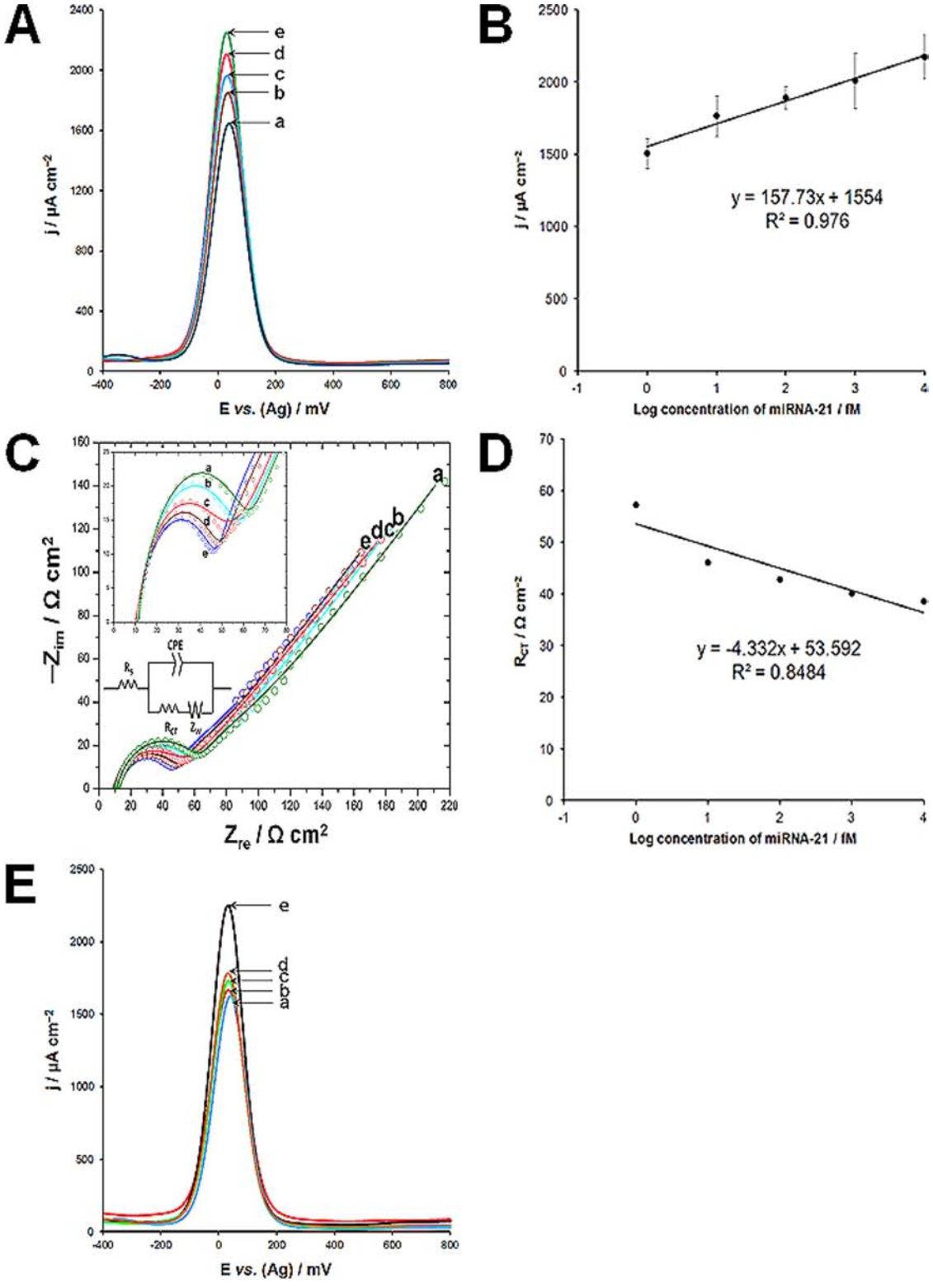

Figure 2. Analytical performance of the hybridization-based sensor (H-SENS). (A) Square wave voltammograms obtained using (a) 1 fM, (b) 10 fM, (c) 100 fM, (d) 1 pM, and (e) 10 pM of miR-21 in the incubation buffer. (B) A calibration plot of current density vs log concentration of miRNA-21. (C) Nyquist plot (—Z_{im} vs Z_{re}) of impedance spectra obtained using (a) 1 fM, (b) 10 fM, (c) 100 fM, (d) 1 pM, and (e) 10 pM of miRNA-21 in the same buffer. The impedance spectra were recorded from 100 kHz to 0.1 Hz, and the amplitude was 0.1 V vs Ag. The inset represents a modified Randles circuit applied to fit to the measured data and consists of the ohmic resistance, R_S, of the electrolyte solution, the electronic charge transfer resistance, R_{CT}, in series with the finite length Warburg W, and in parallel with a constant phase element, CPE. (D) A calibration plot of the resistance to charge transfer (R_{CT}) vs log concentration of miR-21. (E) Selectivity experiments performed using (a) 5.1 mg mL^{-1} HSA, (b) buffer alone, (c) 10 pM of miR-32, (d) 10 pM of miR-122, and (e) 10 pM of miR-21. Electrochemical measurements were performed in the incubation buffer containing 4 mM $K_3[Fe(CN)_6]$ and 10 μM $[Ru(NH_3)_6]Cl_3$.

dx.doi.org/10.1021/ja308216z | J. Am. Chem. Soc. 2013, 135, 3027−3038

shown in Figure 1. The HPD sensor is based on the self-assembly of a thiolated RNA onto gold nanoparticles-modified screen-printed carbon electrode (GNPs-SPGE). This GNPs-SPCE is disposable and commercially available which in turn can allow large-scale production of miRNA profiling chips that can be easily commercialized, taking into account the high stability of short synthetic RNAs. The three-way analysis detects one or multiple miRNAs by a hybridization-based modality (H-SENS), a protein-based modality (P-SENS), and a displacement-based modality (D-SENS). These sensing modalities can be achieved on different electrodes or combined on one electrode (HPD-SENS). In H-SENS, the hybridization of the target miRNA to its complementary immobilized probe causes a modulation of the electrical signal (Figure 1b). Furthermore, addition of the p19 protein dimer to the formed hybrid amplifies the signal and allows an ultrasensitive detection of the target miRNA *via* binding of the bulky p19 protein and consequently shielding the electrode surface (P-SENS, Figure 1c). A universal displacement-based sensor (D-SENS, Figure 1d) is formed on the basis of the self-assembled thiolated RNA probe bound to the saturation concentration of a miRNA, whereas the p19 is attached to the formed hybrid. Subsequently, a mixture of a target miRNA and a nonthiolated RNA probe is incubated with the p19-modified sensor. If the RNA probe is complementary to the miRNA sequence, a newly formed hybrid at relatively higher concentration compared to the concentration of the immobilized hybrid can force the p19 to dissociate from the immobilized hybrid on the electrode surface and to bind to the newly formed hybrid causing a shift-back of the signal. Therefore, this displacement-based sensor can be employed for detection of any type of miRNA without the need of a thiolated capture probe. Square wave voltammetry (SWV) was adopted for miRNA analysis as an effective and rapid technique with well-established advantages, including low detection limits and good discrimination of background currents.[28−30] Furthermore, electrochemical impedance spectroscopy (EIS) was employed to assess the electrochemical results. Notably, EIS is a technique generating a strong interest for analysis of biomolecules because it is label-free and has a less destructive effect on the measured biological interactions since it is usually performed at a very narrow range of small potentials.[31−36]

Hybridization-Based Sensor (H-SENS). Prior to titration experiments, aliquots containing different concentrations of the miR-21 ($^{5'}$pUAGCUUAUCAGACUGAUGUUGA$^{3'}$), including 1 fM, 10 fM, 100 fM, 1 pM, and 10 pM in 30 μL of the incubation buffer were incubated with the probe-modified GNPs-SPCE at 37 °C for 1 h in a dark humidity chamber. SWV was performed at each concentration, and it was observed that the binding between miR-21 and the immobilized capture probe causes an increase in the current density (ON signal). Hence, the modulation of the electrochemical signal was recorded as a function of the current density (j). As shown in Figure 2A, the j value increases linearly with increasing the concentration of miR-21, in the range from 1 fM to 10 pM (corresponding to approximately 10^3 to 10^7 molecules per microliter of sample). A regression equation of $y = 157.73x + 1554$ ($R^2 = 0.976$) was obtained, where y is the j value in μA cm^{-2} and x is the logarithmic concentration of miR-21 in fM, as shown in Figure 2B. The relative standard deviation (RSD) values were between 4% and 8.9%. Beyond the upper miR-21 level, the response became nonlinear, indicating the saturation of the surface with the target molecules. The limit of detection (LOD) was 0.4 fM (7200 molecules per 30 μL of sample), estimated from $3(S_b/m)$, where S_b is the standard deviation of the measurement signal for the blank and m is the slope of the analytical curve in the linear region.[37] In order to confirm the electrochemical finding, a parallel miR-21 analysis was performed using electrochemical impedance spectroscopy (EIS), as shown in Figure 2C. The complex impedance was presented as the sum of the real Z, Z_{re}, and imaginary Z, Z_{im}, components that originate mainly from the resistance and capacitance of the cell, respectively. A suitable equivalent circuit, shown in the inset of Figure 2C, was carefully selected to reflect the real electrochemical process and to enable fit producing accurate values. A modified Randles circuit was used, which consists of the ohmic resistance, R_S, of the electrolyte solution, the electronic charge transfer resistance, R_{CT}, in series with the finite length Warburg, W, and in parallel with a constant phase element, CPE, associated with the double layer and reflecting the interface between the assembled film and the electrolyte solution. The solution resistance, R_S, is the resistance between the probe-modified electrode and the reference electrode. The high frequency semicircle of the Nyquist diagram corresponds to the charge transfer resistance, R_{CT}, in parallel with the CPE. The former represents the electron-transfer kinetics of the redox probe at the electrode surface, whereas the latter corresponds to a nonlinear capacitor accounting for the inhomogeneity of the formed film.[38] The diameter of the semicircle corresponds to the interfacial resistance at the electrode surface, the value of which depends on the dielectric and insulating features of the surface layer. On the other hand, the Warburg impedance, Z_W, accounts for a diffusion-limited electrochemical process, presumably due to molecular motions within the film caused by conducting ions penetration.[39] It was observed that the R_{CT} value decreases linearly with increasing the concentration of miR-21, in the range from 1 fM to 10 pM, with the regression equation of $y = -4.332x + 53.592$ ($R^2 = 0.848$), where y is the R_{CT} value in Ω cm^2 and x is the logarithmic concentration of miR-21 in fM, as shown in Figure 2D and Table S1. Importantly, the high Warburg impedance observed can be attributed to the diffusion of ions through the electrochemically active carbon matrix. As shown in Figure 2E, the selectivity of the developed H-SENS was tested using 10 pM of miR-32 ($^{5'}$pUAUUGCACAUUACUAAGUUGCA$^{3'}$), and it resulted in 16.6% increase in current density (1660.1 μA cm^{-2}) when compared with buffer treatment (0%, 1556.6 μA cm^{-2}) and 10 pM of the target miR-21 (100%, 2197.5 μA cm^{-2}). Furthermore, using 10 pM of miR-122 ($^{5'}$pUGGAGUGUGACAAUGGUGUUUG$^{3'}$) caused 21.6% increase in the j value (1691.4 μA cm^{-2}). Finally, the specificity of the sensor was also tested with 5.1 mg mL^{-1} human serum albumin (HSA, Sigma-Aldrich) which caused 12.9% decrease in j value (1476.3 μA cm^{-2}).

p19 Protein-Based Sensor (P-SENS). Prior to titration experiments, aliquots containing different concentrations of the miR-21 (10 aM, 100 aM, 500 aM, 1 fM, 5 fM, and 10 fM) in 30 μL of the incubation buffer were incubated with the probe-modified GNPs-SPCE at 37 °C for 1 h in a dark humidity chamber. After washing with deionized nuclease-free water, 10 μg mL^{-1} of p19 protein (30 μL) was added to each electrode and incubated at 37 °C for 1 h in a dark humidity chamber. SWV was performed at each concentration, and it was observed that the binding between miR-21 and the immobilized capture probe, followed by incubation with p19 protein, causes a decrease in the current density (OFF signal). Hence, the

dx.doi.org/10.1021/ja308216z | J. Am. Chem. Soc. 2013, 135, 3027−3038

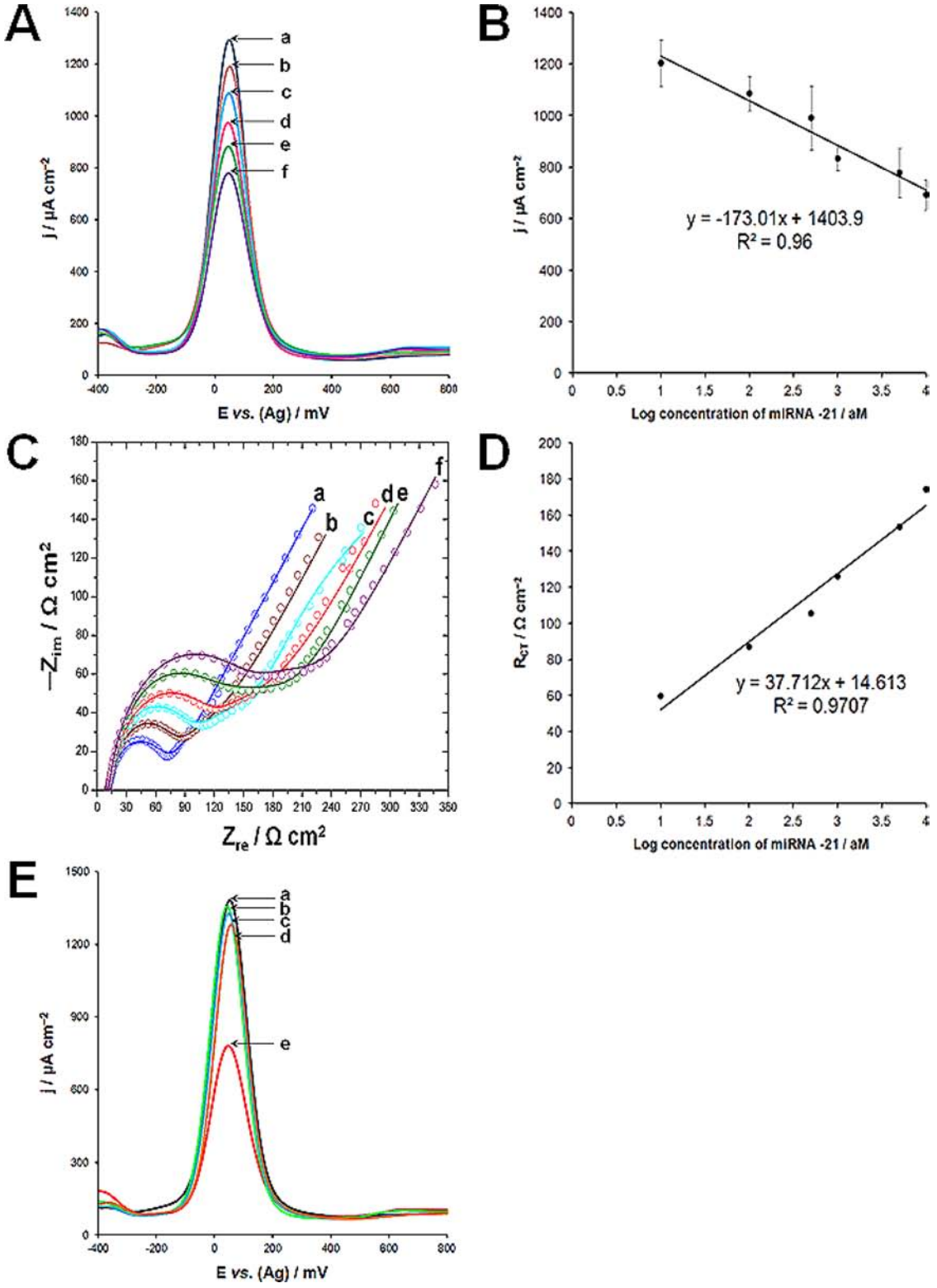

Figure 3. Analytical performance of the p19 protein-based sensor (P-SENS). (A) Square wave voltammograms of the P-SENS obtained using (a) 10 aM, (b) 100 aM, (c) 500 aM, (d) 1 fM, (e) 5 fM, and (f) 10 fM of miR-21 in the incubation buffer, followed by incubation with 10 μg mL^{-1} of p19 protein. (B) A calibration plot of the current density vs log concentration of miR-21. (C) Nyquist plot ($-Z_{im}$ *vs* Z_{re}) of impedance spectra obtained using (a) 10 aM, (b) 100 aM, (c) 500 aM, (d) 1 fM, (e) 5 fM, and (f) 10 fM of miR-21 in the same buffer followed by incubation with 10 μg mL^{-1} of p19 protein. The impedance spectra were recorded from 100 kHz to 0.1 Hz, and the amplitude was 0.1 V vs Ag. (D) A calibration plot of the resistance to charge transfer (R_{CT}) vs log concentration of miR-21. (E) Selectivity experiments performed using (a) buffer alone, (b) 10 fM of miR-32, (c) 5.1 mg mL^{-1} HSA, (d) 10 fM of miR-122, and (e) 10 fM of the target miR-21. Electrochemical measurements were performed in the incubation buffer, containing 4 mM $K_3[Fe(CN)_6]$ and 10 μM $[Ru(NH_3)_6]Cl_3$.

dx.doi.org/10.1021/ja308216z | *J. Am. Chem. Soc.* 2013, 135, 3027−3038

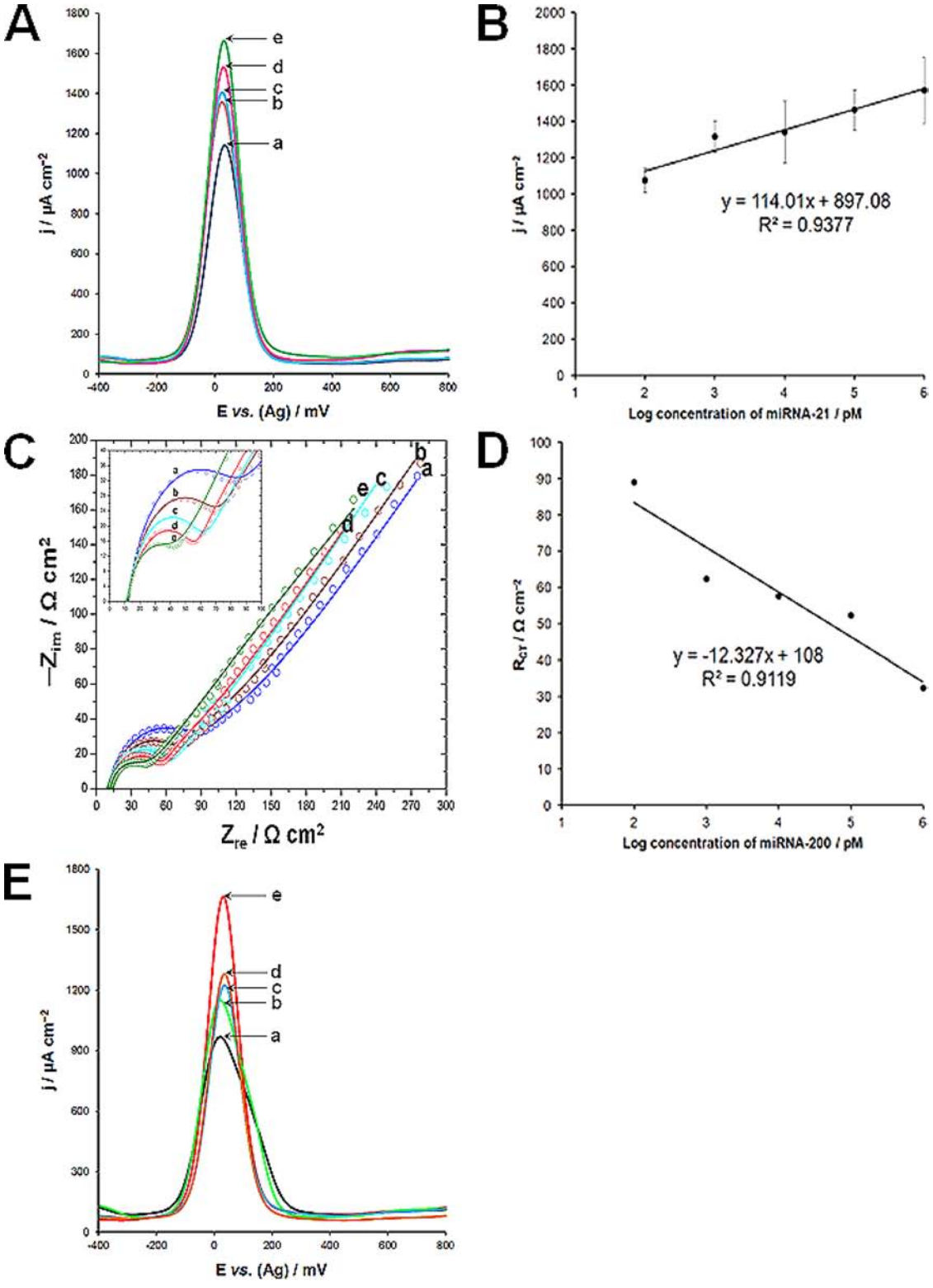

Figure 4. Analytical performance of the displacement-based sensor (D-SENS). (A) Square wave voltammograms of the D-SENS obtained using (a) 100 pM, (b) 1 nM, (c) 10 nM, (d) 100 nM, and (e) 1 μM of the hybridization product of miR-200 and its complementary probe in the incubation buffer. (B) A calibration plot of the current density vs log concentration of miR-200. (C) Nyquist plot ($-Z_{im}$ *vs* Z_{re}) of impedance spectra obtained using (a) 100 pM, (b) 1 nM, (c) 10 nM, (d) 100 nM, and (e) 1 μM of the hybridization product of miR-200 and its complementary probe in the same buffer. The impedance spectra were recorded from 100 kHz to 0.1 Hz, and the amplitude was 0.1 V vs Ag. (D) A calibration plot of the resistance to charge transfer (R_{CT}) vs log concentration of the hybridization product of miR-200 and its complementary probe. (E) Selectivity experiments performed using (a) buffer alone, (b) hybridization product of miR-200 and miR-141 probe, 1 μM each, (c) hybridization product of miR-200 and miR-122 probe, 1 μM each, (d) hybridization product of miR-122 and miR-141 probe, 1 μM each, and (e) hybridization product of miR-200 and its complementary probe, 1 μM each. Electrochemical measurements were performed in the incubation buffer, containing 4 mM $K_3[Fe(CN)_6]$ and 10 μM $[Ru(NH_3)_6]Cl_3$.

dx.doi.org/10.1021/ja308216z | *J. Am. Chem. Soc.* 2013, 135, 3027−3038

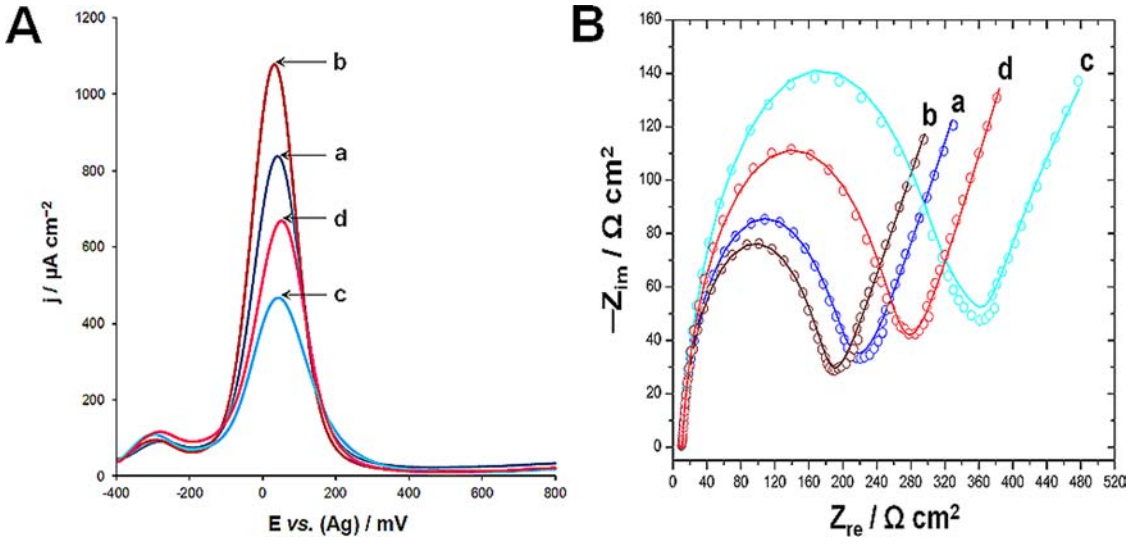

Figure 5. Sequential detection of miR-32 and miR-122 by the HPD sensor. (A) Square wave voltammograms and (B) Nyquist plot ($-Z_{im}$ *vs* Z_{re}) of impedance spectra of the HPD sensor obtained using (a) buffer alone, (b) after incubation with 1 μM of miR-32, (c) after incubation with 10 μg mL^{-1} of p19 protein, and (d) after incubation with the hybridization product of 1 μM of miR-122 and its complementary probe in the incubation buffer. The impedance spectra were recorded from 100 kHz to 0.1 Hz, and the amplitude was 0.1 V vs Ag. Electrochemical measurements were performed in the incubation buffer, containing 4 mM $K_3[Fe(CN)_6]$ and 10 μM $[Ru(NH_3)_6]Cl_3$.

modulation of the electrochemical signal was recorded as a function of the current density (j). As shown in Figure 3A, the j value decreases linearly with increasing the concentration of miR-21, in the range from 10 aM to 10 fM (corresponding to approximately 180 to 18 × 10^4 molecules per 30 μL of sample), with the regression equation of $y = -173.01x + 1403.9$ (R^2 = 0.96), where y is the j value in μA cm^{-2} and x is the logarithmic concentration of miR-21 in aM, as shown in Figure 3B. The relative standard deviation (RSD) values were between 5.4% and 12.2%. Beyond the upper miR-21 level, the response became nonlinear, indicating the saturation of the surface with the target molecules. The LOD was 5 aM (90 molecules per 30 μL of sample). As shown in Figure 3C, parallel EIS measurements showed that the R_{CT} value increases linearly with increasing the concentration of miR-21, within the same range. A regression equation of $y = 37.712x + 14.613$ (R^2 = 0.9707) was obtained, where y is the R_{CT} value in Ω cm^2 and x is the logarithmic concentration of miR-21 in aM, as shown in Figure 3D and Table S2. As shown in Figure 3E, the selectivity of the developed P-SENS was tested using 10 fM of miR-32, and it resulted in 1.5% decrease in current density (1275.6 μA cm^{-2}) when compared with buffer treatment (0%, 1284.5 μA cm^{-2}) and 10 fM of the target miR-21 (100%, 697.3 μA cm^{-2}). Furthermore, using 10 fM of miR-122 caused 14.8% decrease in the j value (1197.7 μA cm^{-2}). Finally, the specificity of the sensor was also tested with 5.1 mg mL^{-1} of HSA, which caused 6.4% decrease in j value (1246.7 μA cm^{-2}).

Displacement-Based Sensor (D-SENS). This sensor was prepared by incubating the miR-21 probe-modified electrode with 30 μL of 1 pM of miR-21 (~100 times higher than the saturation concentration to ensure surface coverage) at 37 °C for 1 h in a dark humidity chamber. After washing, 10 μg mL^{-1} of p19 protein (30 μL) was added to each electrode and incubated at 37 °C for another 1 h in a dark humidity chamber. Prior to titration experiments, aliquots containing different concentrations (100 pM, 1 nM, 10 nM, 100 nM, and 1 μM in 30 μL of the incubation buffer) of the hybridization product of miR-200 ($^{5'}$pUAAUACUGCCUGGUAAUGAUGA$^{3'}$) and its complementary probe ($^{5'}$pCAUCUUACUGGGCAGCAUUGGA$^{3'}$) were incubated with the developed sensor at 37 °C for 1 h in a dark humidity chamber. SWV was performed at each concentration, and it was observed that the added hybridization product forces the p19 protein to dissociate from its complex with the immobilized hybrid causing an increase in the current density (shift-back of signal, ON signal). Hence, the modulation of the electrochemical signal was recorded as a function of the current density (j). As shown in Figure 4A, the j value increases linearly with increasing the concentration of the hybridization product, in the range from 100 pM to 1 μM. A regression equation of $y = 114.01x + 897.08$ (R^2 = 0.9377) was obtained, where y is the j value in μA cm^{-2} and x is the logarithmic concentration of hybridization product in pM, as shown in Figure 4B. The relative standard deviation (RSD) values were between 6.1% and 12.7%. Beyond the upper miR-21 level, the response became nonlinear, indicating the saturation of the surface with the target molecules. The LOD was 50 pM (9 × 10^8 molecules per 30 μL of sample). As shown in Figure 4C, parallel EIS measurements showed that the R_{CT} value decreases linearly with increasing the concentration of the hybridization product, within the same range. A regression equation of $y = -12.327x + 108$ (R^2 = 0.9119) was obtained, where y is the R_{CT} value in Ω cm^2 and x is the logarithmic concentration of the hybrid in pM, as shown in Figure 4D and Table S3. As shown in Figure 4E, the selectivity of the developed D-SENS was tested using 1 μM of the hybridization product of miR-200 and miR-141 probe ($^{5'}$pCAUCUUCCAGUACAGUGUUGGA$^{3'}$), and it resulted in 28.5% increase in current density (1073.3 μA cm^{-2}) when compared with buffer treatment (0%, 875.8 μA cm^{-2}) and 1 μM of miR-200 and its complementary probe (100%, 1567.8 μA cm^{-2}). Additionally, using 1 μM of the hybridization product of miR-200 and miR-122 probe ($^{5'}$pAACGCCAUUAUCACACUAAAUA$^{3'}$) caused 37.8% increase in current density (1137.5 μA cm^{-2}). Furthermore, using 1 μM of the hybridization product of miR-122 and miR-141

dx.doi.org/10.1021/ja308216z | J. Am. Chem. Soc. 2013, 135, 3027−3038

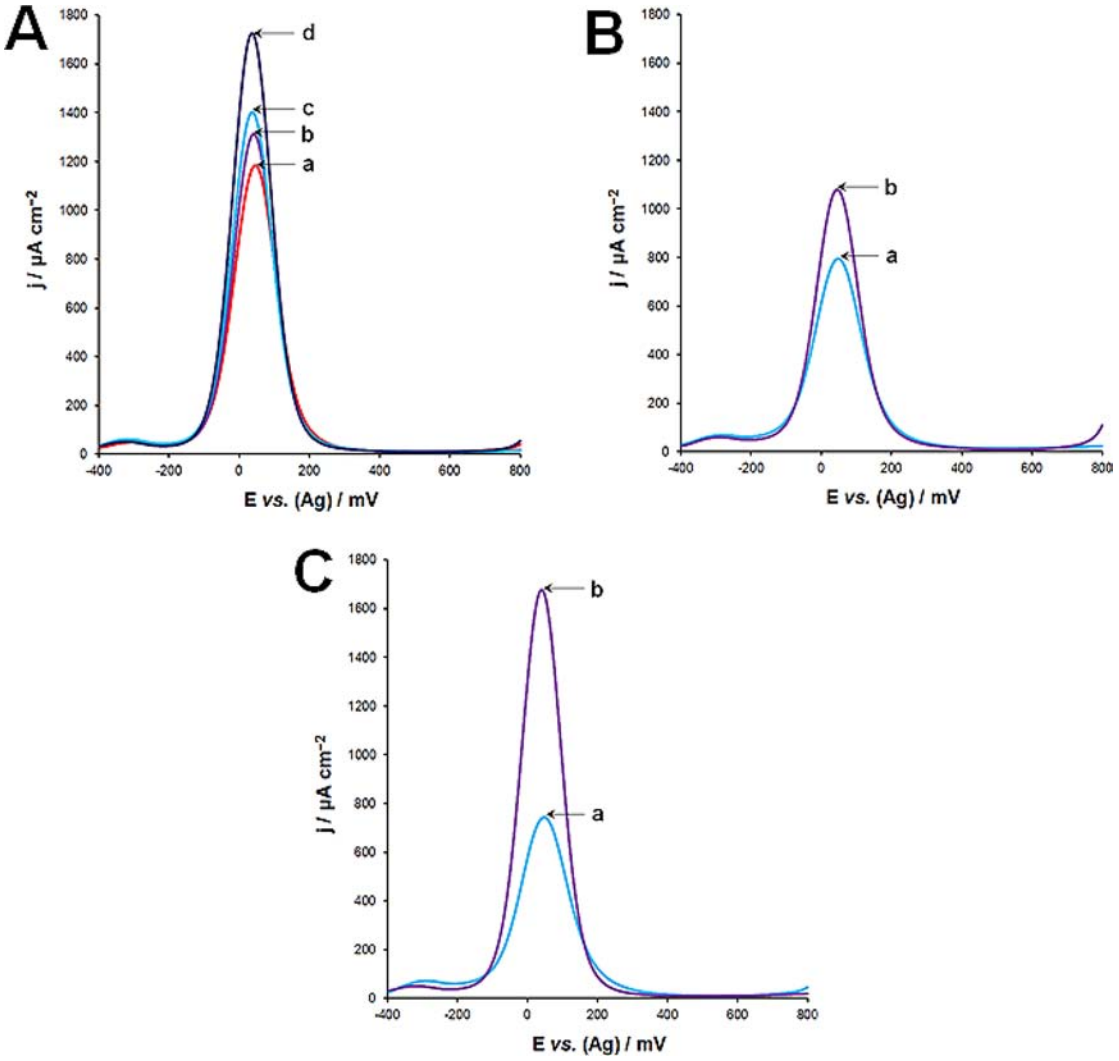

Figure 6. Detection of single-base mismatch and A/U and G/C rich miRNAs. (A) Square wave voltammograms obtained using (a) incubation buffer alone, (b) 10 pM of SBM-T (a terminal mismatch), (c) 10 pM of SBM-M (a middle mismatch), and (d) 10 pM of the fully matched miR-32 in the incubation buffer. (B) Square wave voltammograms obtained using (a) buffer alone, (b) after incubation with 10 pM of A/U rich RNA probe. (C) Square wave voltammograms obtained using (a) incubation buffer alone, (b) after incubation with 10 pM of G/C rich RNA probe. Electrochemical measurements were performed in the incubation buffer, containing 4 mM $K_3[Fe(CN)_6]$ and 10 μM $[Ru(NH_3)_6]Cl_3$.

probe caused 47.4% increase in current density (1204.1 μA cm^{-2}).

Sequential Detection of miR-32 and miR-122 by the HPD Sensor. In an attempt to validate the sensor performance, we completed sequential detection of two different miRNAs (1 μM of miR-32 and miR-122) using the same electrode. The sensing interface consisted of a self-assembled monolayer of 1 μM of the detection probe for miR-32 with the sequence $^{5'}$pUGCAACUUAGUAAUGUGCAAUA$^{3'}$-linker-SH in the incubation buffer for 5 days at 4 °C. This was followed with surface backfilling as previously described in the Experimental Section. As shown in Figure 5A, incubation with miR-32 caused an increase in current density (curve b). After incubation with 10 μg mL^{-1} of p19 protein, there was a large decrease in current density (curve c). Finally, incubation with the hybridization product of the miR-122 and its nonthiolated complementary probe, $^{5'}$AACGCCAUUAUCACACUAAAUA$^{3'}$, caused a shift-back (increase) in current density (curve d). Notably, the added duplex could not fully regenerate the electrode surface presumably due to a side interaction between the sulfur-containing amino acid residues of the p19 protein and the gold surface. A control experiment was performed using the buffer alone (curve a). EIS was carried out in a parallel manner, which corroborated the SWV data, as shown in Figure 5B and Table S4.

Detection of Single Base Mismatches and A/U and G/C Rich miRNAs. The ability of the H-SENS modality to detect single base mismatches was tested. There were 12 sensors utilized, where the first three were incubated with 10 pM of fully matched miR-32 ($^{5'}$pUAUUGCACAUUACUAAGUUGCA$^{3'}$) in 30 μL of the incubation buffer at 37 °C for 1 h in a dark humidity chamber. Three sensors were incubated with 10 pM of miR-32 with a terminal single base mismatch (SBM-T, $^{5'}$pUAUUGCACAUUACUAAGUUGC*G*$^{3'}$, italic letter denotes the mismatch position) and another three were incubated with 10 pM of miR-32 with a single base mismatch at the middle of the strand (SBM-M, $^{5'}$pUAUUGCACAU*U*ACUAAGUUGCA$^{3'}$) in the same buffer. A control experiment was performed by incubating three sensors with the incubation buffer alone. SWV experiments were performed on each sensor. As shown in

dx.doi.org/10.1021/ja308216z | J. Am. Chem. Soc. 2013, 135, 3027−3038

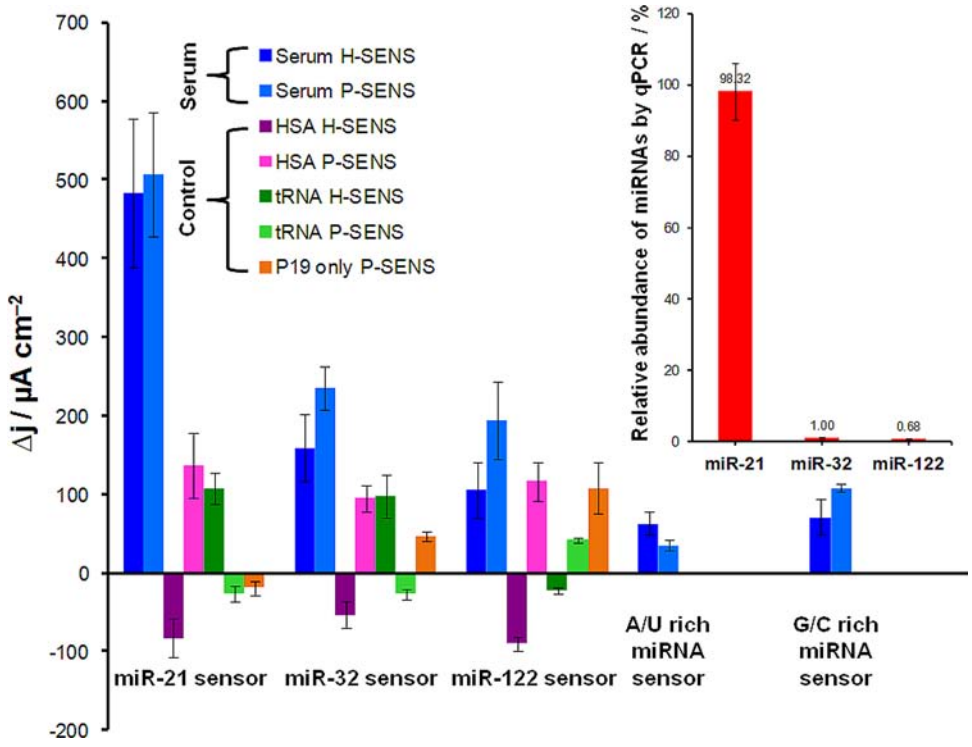

Figure 7. H-SENS and P-SENS profiling of endogenous hsa-miR-21, hsa-miR-32, and has-miR-122 in human serum (dark and light blue columns). Five controls were performed; four of them were carried out by incubating each of the thee sensors with either 5.1 mg mL^{-1} HSA (dark and light violet) or 100 mg mL^{-1} yeast tRNA (dark and light green) followed by incubation with 10 μg mL^{-1} of p19 protein. The fifth control was done by incubating the p19 protein directly with the each of the three sensors under the same incubation conditions (brown columns). In addition, two another sensors containing the A/U and G/C rich probes were tested with the serum aliquot followed by incubation with p19 protein. All SWV experiments were performed in the incubation buffer, containing 4 mM $K_3[Fe(CN)_6]$ and 10 μM $[Ru(NH_3)_6]Cl_3$. The inset presents the relative abundance of hsa-miR-21, hsa-miR-32, and hsa-miR-122 in the same serum sample by qPCR.

Figure 6A, hybridization with SBM-M caused a 40.4% increase in the *j* value (1364.7 μA cm^{-2}), whereas hybridization with SBM-T caused a 22.9% increase in the *j* value (1269.9 μA cm^{-2}). These percentages were calculated by comparison with the buffer treatment alone (0%, 1146.3 μA cm^{-2}) and 10 pM of the fully matched miR-32 (100%, 1686.6 μA cm^{-2}). The results show that the terminal base mismatch causes a larger reduction in electron transfer rate compared to middle base mismatch.

Also, the ability of the H-SENS modality to detect an A/U rich miRNA was tested using three sensors with immobilized $^{5'}$pUAAAACUUAGUAAUGUAUAAUA$^{3'}$-linker-SH onto the sensor surface. The immobilized strand was hybridized with 10 pM of an A/U rich complementary strand [$^{5'}$pUAUUAUACAUUAGUAAUUUUAU$^{5'}$, (90.9% A/U content)] in the same buffer and under the same experimental conditions. A control experiment was performed by incubating three sensors with the incubation buffer alone. On the other hand, the ability of the H-SENS modality to detect a G/C rich miRNA was tested using three sensors with immobilized $^{5'}$pGGCCGCGUCGUAGUGUGCGGUG$^{3'}$-linker-SH onto the sensor surface. The immobilized strand was hybridized with 10 pM of a G/C rich complementary strand [$^{5'}$pGACUGCGCAGGACUCAGUGGCG$^{5'}$, (68.2% G/C content)] in the same buffer and under the same experimental conditions. A control experiment was performed by incubating three sensors with the incubation buffer alone. SWV experiments were carried out on each set of sensors. Interestingly, it was observed that the hybridization with the A/U rich strand caused only 30.9% increase in the *j* value (291.6 μA cm^{-2}, Figure 6B) when compared to hybridization with a G/C rich strand (100%, 942.8 μA cm^{-2}, Figure 6C). This could be attributed to the ability of the G/C rich strand to form a more compact hybrid with the immobilized G/C rich probe causing a higher reduction in the interfacial resistance in contrast with the A/U rich counterpart.

Electrochemical Profiling of miRNAs in Human Serum. We employed both the H-SENS and P-SENS modalities to detect three endogenous circulating miRNAs, including hsa-miR-21, hsa-miR-32, and hsa-miR-122 in human blood serum. Prior to SWV experiments, an excess of yeast tRNA was added to a human serum sample to protect the endogenous miRNAs from nucleases. This was followed by heating a diluted aliquot of one tenth the serum sample in the incubation buffer to release the miRNAs from their inclusions in microparticles and exosomes. SWV experiments showed that the serum level of miR-21 > miR-32 > miR-122, as shown in Figure 7 and Figure S1. The developed sensor was able to profile the abundance of miRNAs and distinguish them from background signals of HSA, yeast tRNA, and p19 alone. In addition, sensors based on either A/U or G/C rich probes did not show any significant binding to the diluted human serum with tRNA. The qPCR analysis of miRNAs in the same serum sample showed similar levels of the three miRNAs and corroborated the sensor data, as seen in the inset of Figure 7. The levels of miRNAs were determined using a standard curve of synthetic miR-32, as shown in Figure S2. Importantly, the levels of miR-32 and miR-122 obtained *via* electrochemical sensing were slightly higher than those obtained by qPCR. This can be ascribed to nonspecific interactions with serum proteins,

dx.doi.org/10.1021/ja308216z | *J. Am. Chem. Soc.* 2013, 135, 3027−3038

yeast RNA, and p19 protein. In addition, these differences also can be attributed to the variation arising from RNA isolation and reactivity of different miRNAs during polyadenilation, reverse transcription, and amplification steps in qPCR experiments. In general, our results ensure that the developed sensor is capable of profiling endogenous miRNAs in serum.

CONCLUSIONS

Implementation of low-cost and commercially available electrochemical sensors in clinical laboratories requires highly sensitive and selective devices. Here, we developed a three-mode electrochemical sensor for miRNA analysis *via* direct hybridization with the target miRNA, p19 protein binding, and protein displacement. Uniquely, the protein displacement sensor (D-SENS) allows the detection of any type of miRNA and eliminates the use of thiolated probes for the target miRNA. The three sensing modalities combined in one HPD sensor link high sensitivity, broad dynamic range of measured concentrations (11 orders of magnitude, from 10 aM to 1 μM), and triple verification of the microRNA concentration. Importantly, the extremely low limit of detection, down to 90 molecules per sample, can be reached without using PCR or any other enzyme-based amplification methods. A single HPD sensor is capable of detecting various miRNAs directly in human blood serum without any preconcentration steps. In addition, the sensor can detect A/U and G/C rich RNAs and distinguish between a fully matched RNA strand and an RNA strand comprising either a terminal or middle single base mutation. Furthermore, the developed sensors are based on nanoparticles-modified screen-printed electrodes that are cheap and commercially available. It opens a new venue for large-scale production of disposable miRNA diagnostics with significant impact on early detection of diseases using biological fluids (blood, saliva, urine, etc.).

ASSOCIATED CONTENT

Supporting Information

Additional figures and tables. This material is available free of charge via the Internet at http://pubs.acs.org.

AUTHOR INFORMATION

Corresponding Author

maxim.berezovski@uottawa.ca

Notes

The authors declare no competing financial interest.

ACKNOWLEDGMENTS

Authors thank the Genomics and Health Initiative of the National Research Council of Canada (J.P.P.), the Natural Sciences and Engineering Research Council of Canada (M.V.B. and J.P.P.), the Early Research Award from the Ministry of Economic Development and Innovation of Ontario (M.V.B.), and Mitacs Elevate Fellowship Program (M.L.) for funding this work.

REFERENCES

(1) Bell, J. *Nature* **2004**, *429*, 453−6.
(2) Walt, D. R. *Science* **2005**, *308*, 217−9.
(3) Baker, M. *Nat. Biotechnol.* **2006**, *24*, 931−8.
(4) Drummond, T. G.; Hill, M. G.; Barton, J. K. *Nat. Biotechnol.* **2003**, *21*, 1192−9.
(5) Lewis, B. P.; Shih, I. H.; Jones-Rhoades, M. W.; Bartel, D. P.; Burge, C. B. *Cell* **2003**, *115*, 787−98.
(6) Lewis, B. P.; Burge, C. B.; Bartel, D. P. *Cell* **2005**, *120*, 15−20.
(7) Nicoloso, M. S.; Spizzo, R.; Shimizu, M.; Rossi, S.; Calin, G. A. *Nat. Rev. Cancer* **2009**, *9*, 293−302.
(8) Gangaraju, V. K.; Lin, H. *Nat. Rev. Mol. Cell Biol.* **2009**, *10*, 116−25.
(9) Cullen, B. R. *Nature* **2009**, *457*, 421−5.
(10) Ambros, V. *Nature* **2004**, *431*, 350−5.
(11) Soleymani, L.; Fang, Z.; Sargent, E. H.; Kelley, S. O. *Nat. Nanotechnol.* **2009**, *4*, 844−8.
(12) Zen, K.; Zhang, C. Y. *Med. Res. Rev.* **2010**, *32*, 326−48.
(13) Lawrie, C. H.; Gal, S.; Dunlop, H. M.; Pushkaran, B.; Liggins, A. P.; Pulford, K.; Banham, A. H.; Pezzella, F.; Boultwood, J.; Wainscoat, J. S.; Hatton, C. S.; Harris, A. L. *Br. J. Haematol.* **2008**, *141*, 672−5.
(14) Nielsen, L. B.; Wang, C.; Sorensen, K.; Bang-Berthelsen, C. H.; Hansen, L.; Andersen, M. L.; Hougaard, P.; Juul, A.; Zhang, C. Y.; Pociot, F.; Mortensen, H. B. *Exp. Diabetes Res.* **2012**, *2012*, 896362.
(15) Laterza, O. F.; Lim, L.; Garrett-Engele, P. W.; Vlasakova, K.; Muniappa, N.; Tanaka, W. K.; Johnson, J. M.; Sina, J. F.; Fare, T. L.; Sistare, F. D.; Glaab, W. E. *Clin. Chem.* **2009**, *55*, 1977−83.
(16) Mitchell, P. S.; Parkin, R. K.; Kroh, E. M.; Fritz, B. R.; Wyman, S. K.; Pogosova-Agadjanyan, E. L.; Peterson, A.; Noteboom, J.; O'Briant, K. C.; Allen, A.; Lin, D. W.; Urban, N.; Drescher, C. W.; Knudsen, B. S.; Stirewalt, D. L.; Gentleman, R.; Vessella, R. L.; Nelson, P. S.; Martin, D. B.; Tewari, M. *Proc. Natl. Acad. Sci. U.S.A.* **2008**, *105*, 10513−8.
(17) Klein, D. *Trends Mol. Med.* **2002**, *8*, 257−60.
(18) Khan, N.; Cheng, J.; Pezacki, J. P.; Berezovski, M. V. *Anal. Chem.* **2011**, *83*, 6196−201.
(19) Russo, M.; Burgyan, J.; Martelli, G. P. *Adv. Virus Res.* **1994**, *44*, 381−428.
(20) Silhavy, D.; Molnar, A.; Lucioli, A.; Szittya, G.; Hornyik, C.; Tavazza, M.; Burgyan, J. *EMBO J.* **2002**, *21*, 3070−80.
(21) Kanaan, Z.; Rai, S. N.; Eichenberger, M. R.; Roberts, H.; Keskey, B.; Pan, J.; Galandiuk, S. *Ann. Surg.* **2012**, *256*, 544−51.
(22) Jalava, S. E.; Urbanucci, A.; Latonen, L.; Waltering, K. K.; Sahu, B.; Janne, O. A.; Seppala, J.; Lahdesmaki, H.; Tammela, T. L.; Visakorpi, T. *Oncogene* **2012**, *31*, 4460−71.
(23) Zhang, Y.; Jia, Y.; Zheng, R.; Guo, Y.; Wang, Y.; Guo, H.; Fei, M.; Sun, S. *Clin. Chem.* **2010**, *56*, 1830−8.
(24) Cheng, H.; Zhang, L.; Cogdell, D. E.; Zheng, H.; Schetter, A. J.; Nykter, M.; Harris, C. C.; Chen, K.; Hamilton, S. R.; Zhang, W. *PLoS One* **2011**, *6*, e17745.
(25) Hu, X.; Macdonald, D. M.; Huettner, P. C.; Feng, Z.; El Naqa, I. M.; Schwarz, J. K.; Mutch, D. G.; Grigsby, P. W.; Powell, S. N.; Wang, X. *Gynecol. Oncol.* **2009**, *114*, 457−64.
(26) Sagan, S. M.; Koukiekolo, R.; Rodgers, E.; Goto, N. K.; Pezacki, J. P. *Angew. Chem., Int. Ed.* **2007**, *46*, 2005−9.
(27) Vargason, J. M.; Szittya, G.; Burgyan, J.; Hall, T. M. *Cell* **2003**, *115*, 799−811.
(28) Labib, M.; Shipman, P. O.; Martić, S.; Kraatz, H.-B. *Electrochim. Acta* **2011**, *56*, 5122−5128.
(29) Labib, M.; Martić, S.; Shipman, P. O.; Kraatz, H. B. *Talanta* **2011**, *85*, 770−8.
(30) Labib, M.; Shipman, P. O.; Martić, S.; Kraatz, H. B. *Analyst* **2011**, *136*, 708−15.
(31) Labib, M.; Zamay, A. S.; Kolovskaya, O. S.; Reshetneva, I. T.; Zamay, G. S.; Kibbee, R. J.; Sattar, S. A.; Zamay, T. N.; Berezovski, M. V. *Anal. Chem.* **2012**, *84*, 8114−7.
(32) Labib, M.; Zamay, A. S.; Muharemagic, D.; Chechik, A.; Bell, J. C.; Berezovski, M. V. *Anal. Chem.* **2012**, *84*, 1677−86.
(33) Labib, M.; Zamay, A. S.; Muharemagic, D.; Chechik, A. V.; Bell, J. C.; Berezovski, M. V. *Anal. Chem.* **2012**, *84*, 2548−56.
(34) Labib, M.; Zamay, A. S.; Muharemagic, D.; Chechik, A. V.; Bell, J. C.; Berezovski, M. V. *Anal. Chem.* **2012**, *84*, 1813−6.
(35) Labib, M.; Zamay, A. S.; Kolovskaya, O. S.; Reshetneva, I. T.; Zamay, G. S.; Kibbee, R. J.; Sattar, S. A.; Zamay, T. N.; Berezovski, M. V. *Anal. Chem.* **2012**, *84*, 8966−9.
(36) Muharemagic, D.; Labib, M.; Ghobadloo, S. M.; Zamay, A. S.; Bell, J. C.; Berezovski, M. V. *J. Am. Chem. Soc.* **2012**, *134*, 17168−77.

(37) Bard, A. J.; Faulkner, L. R. *Electrochemical Methods: Fundamental and Applications*; Wiley: New York, 2001.
(38) Dijksma, M.; Boukamp, B. A.; Kamp, B.; van Bennekom, W. P. *Langmuir* **2002**, *18*, 3105−3112.
(39) Baur, J.; Gondran, C.; Holzinger, M.; Defrancq, E.; Perrot, H.; Cosnier, S. *Anal. Chem.* **2010**, *82*, 1066−72.